Applied Catalysis B: Environmental 259 (2019) 118084

Contents lists available at ScienceDirect

Applied Catalysis B: Environmental

journal homepage: www.elsevier.com/locate/apcatb

Efficient bifunctional piezocatalysis of Au/$BiVO_4$ for simultaneous removal of 4-chlorophenol and Cr(VI) in water

Yan Wei, Yiwen Zhang, Wei Geng, Hanrui Su, Mingce Long*

School of Environmental Science and Engineering, Key Laboratory of Thin Film and Microfabrication Technology (Ministry of Education), Shanghai Jiao Tong University, 800 Dongchuan Road, Shanghai 200240, China

ARTICLE INFO

Keywords:
Piezocatalytic effect
Gold modified bismuth vanadate
Bifunctional catalysis
Hydrogen peroxide
Ultrasonic vibration

ABSTRACT

Piezocatalysis induced by polarization of piezoelectric materials is considered as an emerging technology in environmental cleanup. In this work, a piezoelectric material, Au nanoparticles modified $BiVO_4$ (Au/$BiVO_4$) is synthesized and its piezoelectric response is observed by piezo-response force microscopy. Au/$BiVO_4$ is used as a bifunctional piezocatalyst for simultaneous removal of 4-chlorophenol (4-CP) and hexavalent chromium (Cr(VI)) upon ultrasonic vibration, with 91% and 83% of removal efficiency in 120 min, respectively. The piezocatalytic performance of Au/$BiVO_4$ increases with the increase of ultrasonic power and the decrease of pH. The main active species for 4-CP oxidation and Cr(VI) reduction are determined to be $^{\cdot}OH$ and H_2O_2, respectively, since a significant formation rate of $^{\cdot}OH$ is estimated by a probe method, and a high amount of H_2O_2 accumulation is directly detected. This study provides understanding on the piezocatalysis mechanism and brings new insights for development of piezocatalysis for multifunctional environmental applications.

1. Introduction

Piezoelectricity is a phenomenon to generate electrical potentials in piezoelectric materials when there is mechanical deformation on them [1,2]. This effect has been widely applied in actuators, sensors, and voltage generators [3,4]. Piezocatalysis is an emerging technology to employ the materials with piezoelectric effect to remove recalcitrant organic pollutants. When the piezoelectric materials are subjected to an external mechanical stress, such as ultrasonic vibration, polarization charges with opposite polarities will be generated and subsequently separate and migrate to the polar surfaces and form an internal electric field. The electric field can promote the separation of free electrons and holes in the materials, and generate active species for redox reactions [2,5–7]. Due to the great potential in dealing with environmental issues by utilizing the low cost mechanical energy, piezocatalysis has attracted increasing interests in the field of advanced oxidation processes.

Currently, several materials with piezoelectric effect has been investigated as piezocatalysts for pollutant removal. $BaTiO_3$ is the most intensively studied one, which exhibits capability of organic contaminants decomposition [8–10] and water splitting [11] under ultrasonic vibration. Other perovskite-type piezocatalysts such as $BiFeO_3$ [12], $NaNbO_3$ [13], $PbTiO_3$ [14] and $ZnSnO_3$ [15] have also been investigated to some extent. Besides, piezocatalysis is often coupled with photocatalysis, i.e. piezo-photocatalysis, to enhance the catalytic activity [16]. For instance, ZnO is widely used as a piezo-photocatalyst for organic dye removal, due to its semiconducting characteristic [17]. Other piezocatalytic materials with special morphologies, for example, MoS_2 nanosheets [18,19] and BiOCl microplates [20] have also been studied. However, the development of piezocatalysts is still in its infancy. Development of effective and stable piezocatalystic materials is the basic requirement for the study and application of piezocatalysis.

On the other hand, the co-existence of organic compounds and inorganic heavy metal ions in wastewater has become a common phenomenon with the rapid development of industry and agriculture [21,22]. These organic and inorganic pollutants, for instance, 4-chlorophenol (4-CP) and hexavalent chromium (Cr(VI)), are always highly toxic and can damage human health and living beings [2,23–26]. However, to the best of our knowledge, the current researches on piezocatalysis are normally target on the degradation of a single organic pollutant in wastewater, especially dyes, ignoring either the co-existence of heavy metals ions or organic pollutants [5,27]. Since piezocatalysis processes can separate free electrons and holes on the surface of catalysts, which can both act as active species for reduction and oxidation, respectively. Therefore, piezocatalysis has great potential for energy-efficient and time-saving bifunctional applications, including reduction of heavy metal ions and oxidation of organic pollutants.

$BiVO_4$ is a popular photocatalyst for water splitting and organic pollutant degradation under visible light irradiation due to its proper

* Corresponding author at: School of Environmental Science and Engineering, Shanghai Jiao Tong University, 800 Dongchuan Road, Shanghai 200240, China.
E-mail address: long_mc@sjtu.edu.cn (M. Long).

https://doi.org/10.1016/j.apcatb.2019.118084
Received 3 July 2019; Received in revised form 11 August 2019; Accepted 13 August 2019
Available online 15 August 2019
0926-3373/

band gap (E_g ~ 2.4 eV) [28–30]. Simultaneously, due to its inherent ferroelectricity, $BiVO_4$ possesses piezoelectric performance and has the potential to be used as a piezocatalyst [31,32]. However, as far as we know, no research on piezocatalysis of $BiVO_4$ has been reported, which could be ascribed to its weak piezoelectric performance. Loading Au nanoparticles on the surface of piezocatalysts is an effective strategy to enhance piezocatalytic activity due to the enhancement of free charges separation [33,34]. In this study, a piezocatalyst, Au nanoparticles modified bismuth vanadate (Au/$BiVO_4$), was synthesized by a urea assisted deposition-precipitation method, which displayed a highly efficient piezocatalytic effect and was employed as a bifunctional catalyst for simultaneous removal of 4-CP and Cr(VI) in water. Furthermore, the mechanism on the piezocatalytic-based bifunctional catalysis was revealed.

2. Experimental section

2.1. Preparation of catalysts

Monoclinic $BiVO_4$ was prepared in aqueous medium by a previous reported method [35]. Briefly, 80 mmol $Bi(NO_3)_3$ and 80 mmol NH_4VO_3 were dissolved in a 200 mL HNO_3 (1.84 M) solution, respectively. After stirring for 0.5 h, the two solutions were mixed with the addition of 15 g urea, and then was stirred for 8 h at 90 °C. The precipitates were filtered, washed, and dried at 60 °C.

Au/$BiVO_4$ catalysts were prepared via a deposition-precipitation method in a hot urea solution [36]. In a typical synthesis, 0.5 g $BiVO_4$ was dispersed into a 50 mL urea (0.42 M) solution. The mixture was ultrasonically treated for 15 min, and followed by the addition of 1.08 mL $HAuCl_4$ (10 g/L) aqueous solution. After sonication for another 15 min, the solution was stirred vigorously at 90 °C for 4 h. The precipitates were collected, washed with deionized water, and calcined at 300 °C for 2 h at a rate of 2 °C min^{-1} to turn the Au(III) complexes into metallic gold nanoparticles. If not specified, Au/$BiVO_4$ in the following text refers to Au/$BiVO_4$ with an Au loading content of 1.0 wt%. Au/$BiVO_4$ with different Au loading contents (0.25%, 0.5%, and 2%) were synthesized according to the same method, except that the amount of $HAuCl_4$ addition was different.

2.2. Characterization

The crystal phase of catalysts was analyzed by X-ray diffraction (XRD, D/max-2200/PC, Rigaku) with Cu Kα radiation as a monochromatized source at 40.0 kV and 30.0 mA (λ = 0.154 nm). The morphologies of Au/$BiVO_4$ were identified by scanning electron microscopy (SEM, S-4800, Hitachi) and transmission electron microscopy (TEM, G2F20, TECNA1). The elemental mapping images were obtained from TEM equipped with an energy dispersive X-ray spectroscopy (EDS). X-ray photoelectron spectroscopy (XPS) data were obtained using an AXIS Ultra DLD system (Shimadu-Kratos Company) and the binding energies were normalized with the signal for carbon (C_{1S} = 284.6 eV) as a reference. The piezoelectric response of as-prepared sample was characterized by a piezoresponse force microscopy (PFM), which is an atomic force microscope (AFM, Dimension Icon & FastScan Bio, Bruker) equipped with a ferroelectric test system. The electron paramagnetic resonance (EPR) spectra of superoxide radicals ($O_2^{\cdot -}$) adducts were gained by using a Bruker ELEXSYS 580 spectrometer. The microwave power, modulation amplitude and microwave frequency were set at 10 mW, 2.0 G and 9.81 GHz, respectively. 5-tert-Butoxycarbonyl-5-methyl-1-pyrroline-N-oxide (BMPO) was used as a spin-trapping agent.

2.3. Piezocatalytic performance

The bifunctional piezocatalytic activity of Au/$BiVO_4$ was evaluated by the simultaneous removal of 4-CP and Cr (VI) under ultrasonic vibration. In a typical test, 25 mg catalyst was added into a 50 mL of solution containing 0.1 mM 4-CP and 10 mg/L Cr (VI). Prior to the ultrasonic vibration, the suspension was continuously stirred for 30 min to reach an adsorption equilibrium, and then ultrasonic vibration was carried out in an ultrasonic cleaner (KQ-300DE, Kunshan Ultrasonic Instrument) with a frequency of 40 kHz and a power of 120 W. The reaction system was kept around 25 °C. At specified time intervals, 1.5 mL of sample was withdrawn and filtered through a 0.22 μm membrane filter.

The concentration of 4-CP was analyzed by using a HPLC (Shimadzu LC-2010AHT) equipped with a Shim Pack C18 chromatographic column (ZORBAX Eclipse XDB-C18) and an UV–vis detector (SPD-20AV). Detailed HPLC analytical parameters including mobile phase, flow rate, and detection wavelength are shown in **Table S1**. The concentration of Cr(VI) was determined by a diphenylcarbazide method with a UV–vis spectrophotometer (WFJ-7200, UNIC) at λ = 540 nm [37]. The concentration of H_2O_2 was tested by using a modified DPD–POD method [38].

3. Results and discussion

3.1. Characterization of catalysts

The crystal structure of as-prepared catalysts was verified by XRD analyses (Fig. 1a). The diffraction peaks of $BiVO_4$ and Au/$BiVO_4$ are corresponded to the standard card of monoclinic $BiVO_4$ (JCPDS No. 14-0688). No observable change in the crystal structure after being modified by a low content of Au nanoparticles [39]. XPS spectra were also carried out to investigate the surface chemical composition and elementary valent state of Au/$BiVO_4$ (**Fig. S1**). The characteristic peaks at 84.0 and 87.7 eV in the XPS spectrum of Au 4f can be ascribed to Au $4f_{7/2}$ and Au $4f_{5/2}$ of Au^0 species, respectively. This confirms the existence of Au nanoparticles on the surface of the composite [40]. An insight into the microstructure of the as-prepared Au/$BiVO_4$ was examined by SEM and TEM characterizations. As shown in Fig. 1b, Au nanoparticles with a size of 5–15 nm are homogeneously distributed on the surface of $BiVO_4$. The successful loading of Au nanoparticles on $BiVO_4$ is also confirmed by TEM images (Fig. 1c). A HRTEM image collected from the Au/$BiVO_4$ reveals that the lattice fringes on the small dots in the edge of particles has an interplanar spacing of 0.23 nm (Fig. 1d), which is assigned to Au (111) plane [39]. EDS mapping images (Fig. 1e) clearly reveal the distribution of Au, Bi, V and O, demonstrating that the Au nanoparticles are homogeneously deposited on the $BiVO_4$.

The piezoelectric property of Au/$BiVO_4$ was confirmed by PFM measurements. A localized point to point piezo-response was studied by applying a bias voltage on a conductive cantilever tip. The PFM phase and amplitude images for Au/$BiVO_4$ are shown in Fig. 2a and b. A phase contrast among different regions of Au/$BiVO_4$ can be observed, indicating the existence of different polarization directions. The clear contrast of amplitude image (Fig. 2b) also suggests the presence of distinct and randomly distributed ferroelectric domains [41]. The phase angles exhibit a ~ 180° change under the reversal of a 10 V potential (Fig. 2c), indicating the local switching of the ferroelectric polarization in the Au/$BiVO_4$ particles [42,43]. Moreover, the clear "butterfly shape" amplitude loop (Fig. 2d), which is a well-established characteristic of ferroelectric materials, also proves the ferro-/piezoelectric nature of Au/$BiVO_4$ [13].

3.2. Bifunctional piezocatalytic performance

The 4-CP and Cr(VI) mixed solutions were used to evaluate the bifunctional catalytic performance of Au/$BiVO_4$ in the simultaneous removal of refractory organics and heavy metals. The essential role of piezoelectricity in the catalytic process was demonstrated by comparing 4-CP degradation and Cr(VI) reduction under different conditions: with

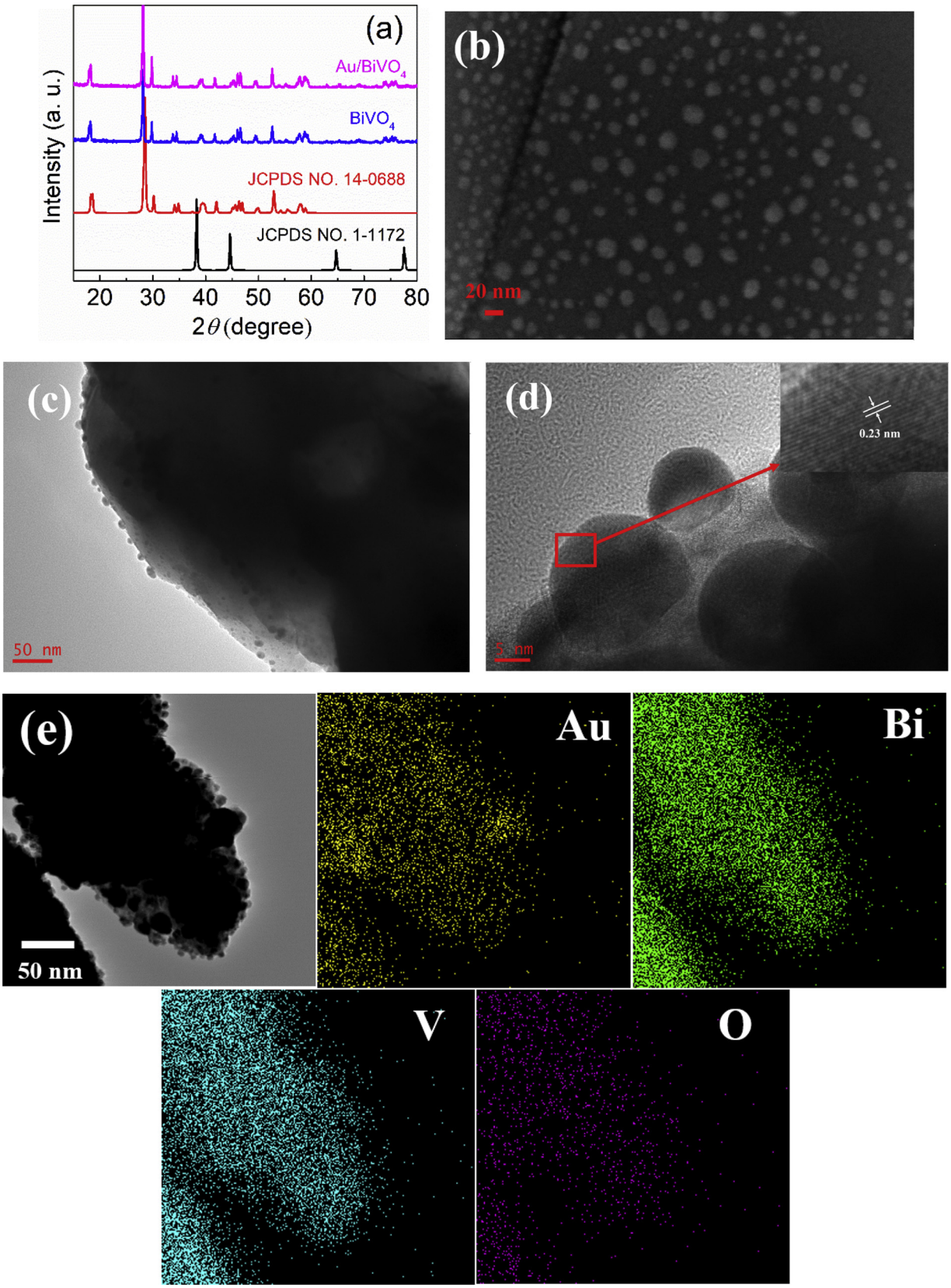

Fig. 1. (a) XRD patterns of $BiVO_4$, $Au/BiVO_4$, and standard data of monoclinic $BiVO_4$ (JCPDS No. 14-0688) and cubic gold (JCPDS No. 1-1172); (b) SEM; (c and d) TEM images; (e) TEM and EDS mapping of $Au/BiVO_4$.

catalysts only, with ultrasound (US) only, and with both. As shown in Fig. 3a and b, remarkable 4-CP degradation and Cr(VI) reduction (91% and 83% in 120 min, respectively) are achieved with the simultaneous existence of ultrasonic vibration and $Au/BiVO_4$. However, the removal of 4-CP and Cr(VI) are negligible in the absence of either $Au/BiVO_4$ or ultrasonic energy. The result excludes the possibility of direct

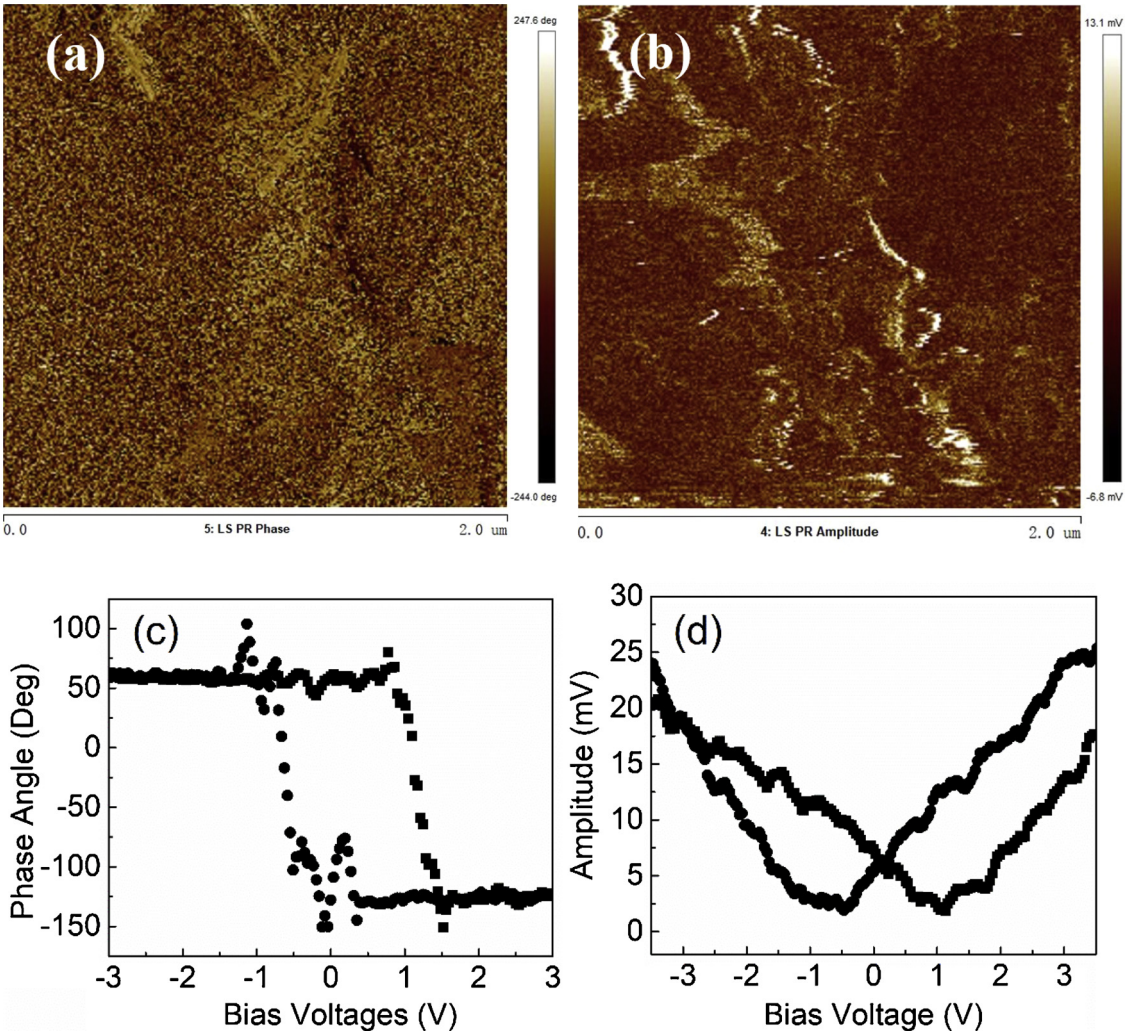

Fig. 2. (a) The relative phase of the piezoelectric response; (b) the amplitude of the piezoelectric response; (c) phase hysteresis loop and (d) amplitude butterfly loop for Au/$BiVO_4$.

contaminants removal by ultrasound or adsorption, while the simultaneous removal of 4-CP and Cr(VI) may be ascribed to piezocatalytic effect of Au/$BiVO_4$ that was also proved by PFM results. Moreover, the bifunctional catalytic performance of Au/$BiVO_4$ for removing 4-CP and Cr(VI) is comparable to that of reported catalysts in photocatalysis and piezocatalysis (**Table S2**), confirming the potential of Au/$BiVO_4$ in bifunctional piezocatalytic applications [2,21,26,44–46].

To determine the effect of Au loading, the catalytic performance of pure $BiVO_4$ was also compared (Fig. 3a and b). As a result, pure $BiVO_4$ exhibits a poor catalytic activity with only 44% 4-CP degradation and 24% Cr(VI) reduction after 120 min reaction. This result indicates that the loading of Au nanoparticles on $BiVO_4$ plays an important role in the enhancement of piezocatalytic activity, since Au nanoparticles on the surface of $BiVO_4$ can act as the sites to trap electrons and effectively improve the separation efficiency of electrons and holes [33,34]. The removal of 4-CP and Cr(VI) by Au/$BiVO_4$ with different Au loading contents were shown in Fig. 3c and d. Since Au precursor concentration has little effect on the size of Au nanoparticles (**Fig. S2**) [47], the effect of Au nanoparticle size on the catalytic performance of Au/$BiVO_4$ with different Au loading can be excluded. The removal efficiency of Au/$BiVO_4$ increases with the increase of Au contents, and reaches the highest point at 1 wt% loading of Au nanoparticles. However, the activity decreases with the Au content above 1 wt%. The declined performance can be attributed to that excess Au nanoparticles may cover the active sites on the surface of $BiVO_4$ and hinder the migration of charge carriers [39].

Effect of oxygen on piezocatalytic performance of Au/$BiVO_4$ was explored. As shown in Fig. 4a and b, the removal of 4-CP (15%) and Cr (VI) (12%) is insignificant in N_2 atmosphere. It is worth noting that electrons are the only active species that can reduce Cr(VI) in nitrogen atmosphere. Thus it can be inferred that only 12% of the Cr(VI) reduction is achieved in 120 min through a direct electron acquisition pathway, and it is a very slow process. This result also indicates that O_2 plays an indispensable role in the Au/$BiVO_4$ piezocatalytic system. Generally, the active species like $O_2^{\cdot -}$ and H_2O_2 can be generated from oxygen reduction reaction during the piezocatalytic process [20]. Therefore, the critical role of O_2 in Au/$BiVO_4$ piezocatalytic system may be related to the scavenging of free electrons and formation of active species.

The synergistic removal of 4-CP and Cr(VI) was proved through the piezocatalytic tests on their single and co-existed solutions. The mixture system with both pollutants exhibits a higher removal efficiency than those with a single pollutant (Fig. 4c and d). The synergistic effect in 4-CP and Cr(VI) removal also highlights the bifunctional performance of Au/$BiVO_4$ piezocatalysis. For Cr(VI) reduction, the reduction efficiency increases significantly from 60% to 87% in the presence of 4-CP, which is may due to the accelerated electron-hole separation in the piezocatalyst with the co-existing organics [48]. However, the presence of Cr (VI) has little effect on 4-CP removal (**Fig. S3**), suggesting that the existence of Cr(VI) cannot obviously promote electron-hole separation

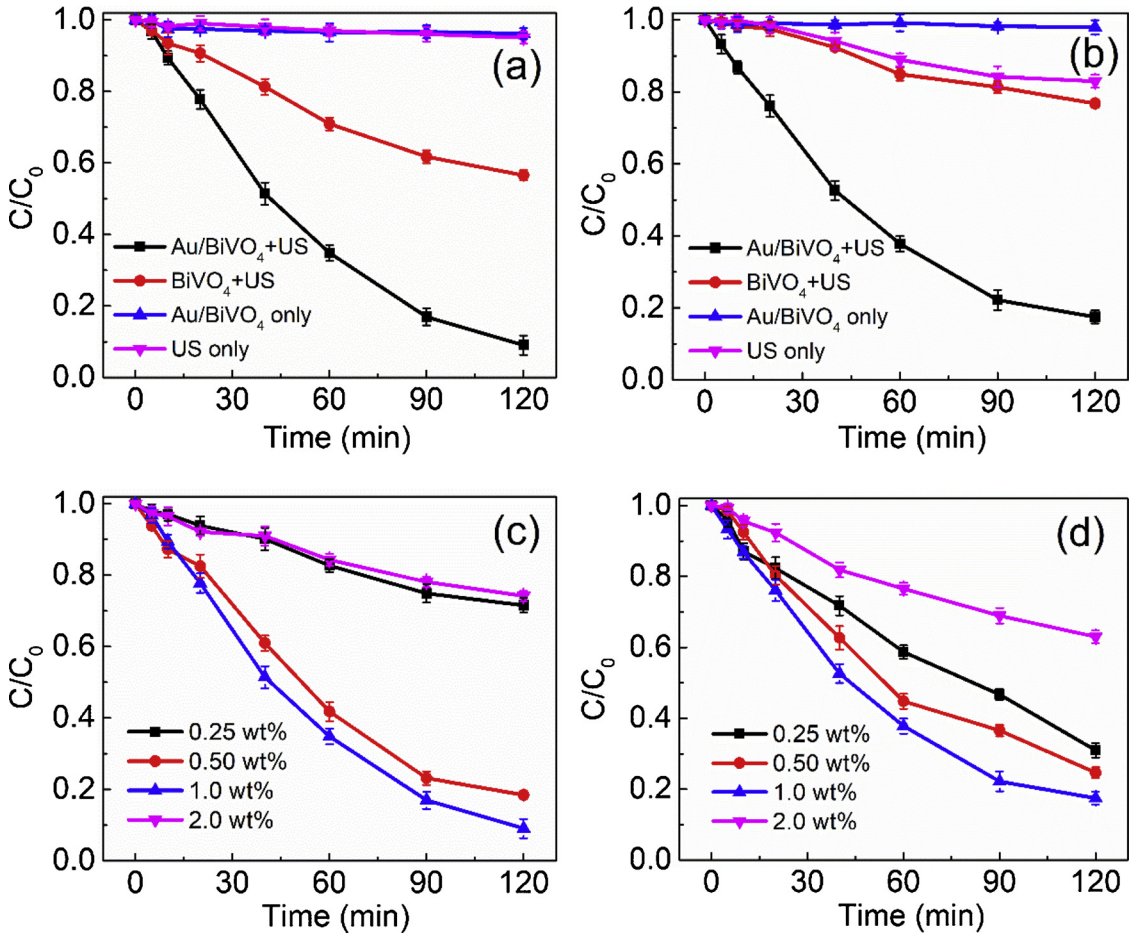

Fig. 3. The removal of 4-CP (a and c) and Cr(VI) (b and d) in different processes (a and b), and effect of Au contents in $Au/BiVO_4$ (c and d).

and 4-CP degradation. This is consistent with the results of Cr(VI) reduction in the absence of oxygen, and proves the directly reduction of Cr(VI) by free electrons generated from the catalyst is slow and low efficiency.

The effects of reaction parameters on 4-CP and Cr(VI) removal in the $Au/BiVO_4$ piezocatalytic system were investigated. As shown in Fig. 5a and b, with the increase of ultrasonic vibration powers, the removal efficiencies (at 120 min) of 4-CP and Cr(VI) gradually increased from 59% and 53% (80 W) to 100% and 94% (300 W), respectively. The enhanced piezocatalytic performance can be explained by Eq. (1) [18,49],

$$V_P = (\tau_n d_{xn} W_x)/(\varepsilon_{rx}\varepsilon_0) \quad (1)$$

wherein V_P represents the piezopotential, τ_y is the applied stress in the y dimension, d_{xy} is the piezoelectric coefficient, W_x is the width of piezoelectric material in the x dimension, ε_{rx} is the relative permittivity in the x dimension, and ε_0 refers to the electrical permittivity of free space. Thus, a higher ultrasonic power, which leads to a higher applied stress (τ_y) on $Au/BiVO_4$, can generate a stronger piezoelectric field (V_P), so as to facilitate the removal of contaminants. When the dosage of $Au/BiVO_4$ increases from 0.25 g/L to 0.75 g/L, the removal efficiency of contaminants increases gradually due to the higher catalyst dosage can provide more active sites (Fig. 5c and d). However, the removal efficiency began to decline as the dosage of catalyst further increases to 1.0 g/L. This is may be ascribed to the aggregation of excess $Au/BiVO_4$ particles, which cause the decrease in the number of the active sites on the surface of $Au/BiVO_4$ [50]. To investigate the effect of temperature on contaminant removal, experiments were conducted at three different temperatures (25, 35 and 45 °C). As shown in Fig. 5e and f, when the temperature increased from 25 °C to 35 °C, the removal efficiency of 4-CP and Cr(VI) are significantly enhanced, achieving 100% in 120 min. However, with the temperature increases to 45 °C, the catalytic activity of $Au/BiVO_4$ decreases significantly. This can be ascribe to the apparent decrease of dissolved oxygen concentration in the aqueous solution, which is decreased from 8.3 mg/L (25 °C) to 5.9 mg/L (45 °C). As mentioned above, oxygen displays a critical role in $Au/BiVO_4$ piezocatalytic system for contaminant removal (Fig. 4a and b). The effect of the initial pH was investigated by adjusting the solution pH using 1 M NaOH and 1 M HNO_3. Moreover, the influences of Na^+ and NO_3^- from NaOH and HNO_3 to contaminant removal are excluded by evaluating the effect of $NaNO_3$ (**Fig. S4**). As shown in Fig. 5g, 4-CP degradation efficiency is improved under acidic conditions, with almost completely removal in 120 min. This phenomenon can be explained by enhanced adsorption capacity of 4-CP on the catalyst, which was 5.5%, 4.5% and 4.0% for pH at 3.6, 6.6 and 9.9, respectively. Moreover, the generated electrons are more prone to interact with positively charged protons under acidic conditions, which results in a higher separation efficiency of electrons and holes [51]. Similarly, Cr(VI) reduction performance of the $Au/BiVO_4$ piezocatalytic system is better when pH value is lower (Fig. 5h). Since when pH = 3.6, the major species of Cr(VI) are $HCrO_4^-$, CrO_4^{2-} and $Cr_2O_7^{2-}$ ions, and that existence of abundant H^+ could be beneficial to reduction of Cr(VI) oxions, while the presence OH^- would inhibit it [51,52].

Furthermore, both chloride and sulfate anions have little effect on the removal of 4-CP and Cr(VI) (**Fig. S5**). When other organic substances, like benzoic acid and phenol, are used to replace 4-CP, the $Au/BiVO_4$ piezocatalytic system can also remove organics and Cr(VI) effectively (**Fig. S6**). It suggests that $Au/BiVO_4$ piezocatalysis exhibits a potential for application in a wide range due to its resistance to anions in water and applicability of multiple pollutants.

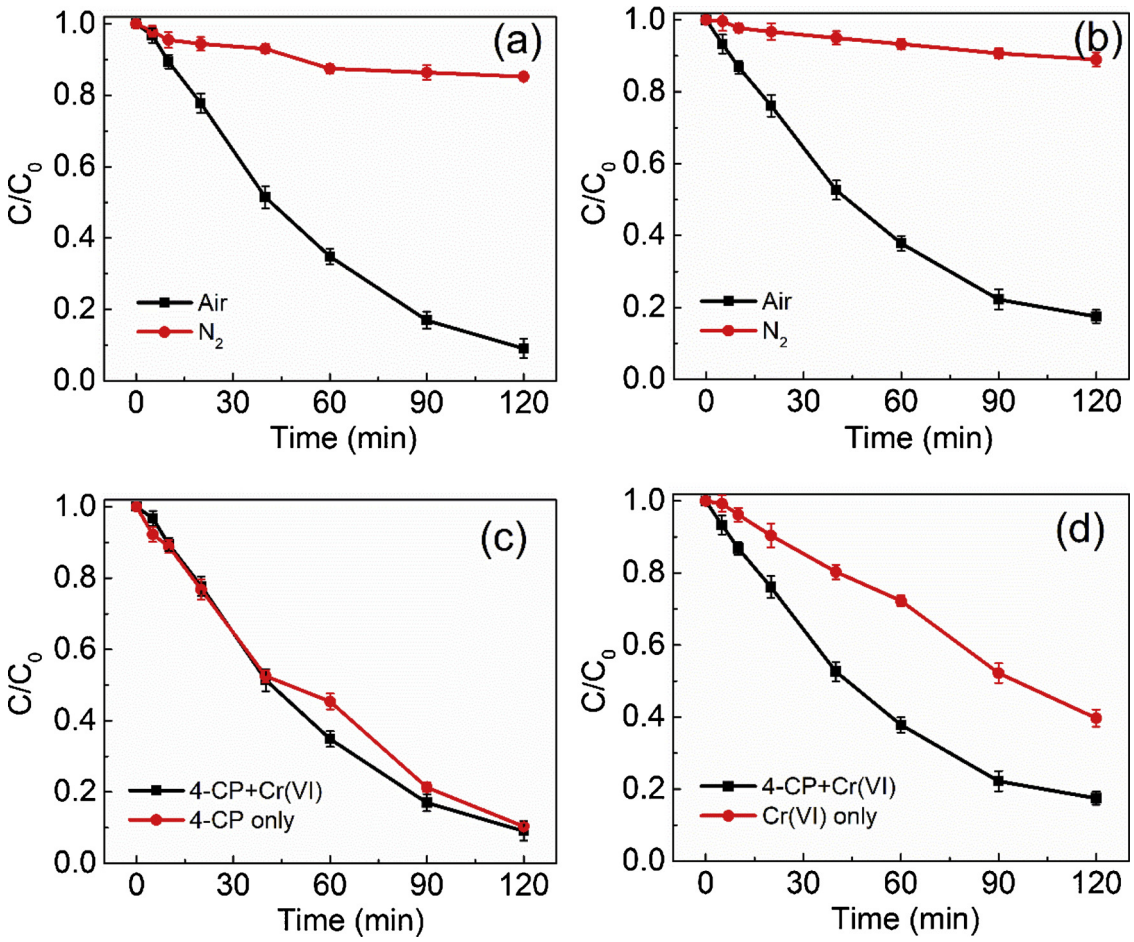

Fig. 4. The removal of (a and c) 4-CP and (b and d) Cr(VI) in different atmosphere (a and b) and in single and co-existed solution (c and d).

The stability of $Au/BiVO_4$ was evaluated by cycle experiments (Fig. 6). About 75% of 4-CP and 70% of Cr(VI) can be removed in the third run, indicating a reliable stability of this catalytic system. The slightly decreased catalytic activity of $Au/BiVO_4$ is probably due to the adsorption of intermediates, which is proved by comparing the XPS spectra of $Au/BiVO_4$ after reaction and the fresh one (**Fig. S1**). The binding energy at about 531.4 eV corresponds the adsorbed oxygen containing species on the catalyst [53,54], which increases after the reaction (**Fig. S1c**), indicating the adsorption of the oxygen-containing intermediates on the surface of the catalyst. On the other hand, the Bi 4f binding energies of $Au/BiVO_4$ after reaction exhibit slightly blue shift (**Fig. S1a**), which was probably due to the slight increase in the sizes of Au nanoparticles after the reaction [40]. The XRD pattern of $Au/BiVO_4$ after reaction shows little change compared with that of the fresh one (**Fig. S7a**), indicating the unchanged crystal structure of $Au/BiVO_4$. The SEM and TEM images show that Au nanoparticles are still homogeneously distributed on the surface of $BiVO_4$ (**Fig. S7b – 7d**). The sizes of most Au nanoparticles are still between 5–15 nm, with only a few nanoparticles growing to around 20 nm. This is consistent with the blue shift of the XPS spectra of Bi 4f mentioned above. In general, the microstructure of $Au/BiVO_4$ after reaction also exhibits negligible change, further reflecting the stability of the catalyst.

3.3. Mechanism discussion

Generally, the "hot spot" produced by ultrasonic cavitation effect in water medium can reach a very high temperature (about 5000 °C) [55]. Such a high temperature can make $BiVO_4$ particles generate free electrons and holes, which would migrate to the surface and lead to formation of active species [6,56]. Au nanoparticles, which act as active sites for electrons trapping, can effectively decrease recombination of electron-hole pairs [33,34]. At the same time, the ultrasonic vibration can induce $Au/BiVO_4$ to produce piezoelectric polarization and generate an internal electric field due to the piezoelectric nature. As shown in Scheme 1, the generated internal electric field can attract free electrons and holes within $Au/BiVO_4$ towards opposite directions and accumulate on the surface of the crystal. Simultaneously, both of the conduction band (CB) and valence band (VB) of $Au/BiVO_4$ will be tilted due to the piezoelectric potential, which can further facilitate the migration of free charges [5,43].

In order to identify the active species during piezocatalytic process, TBA was used as a probe of ·OH [57]. As shown in Fig. 7a, the presence of TBA dramatically inhibits 4-CP degradation, indicating the presence of ·OH. Various dosage of TBA was added into the system to probe the formation rate of ·OH. On the basis of a steady-state approximation of ·OH, the degradation rates of 4-CP (R^{d}_{4-CP}, M s^{-1}) can be calculated according to Eq. (2) [58], where $R^{f}_{\cdot OH}$ represents the formation rate of ·OH, $k_{4-CP,\cdot OH}$ ($7.6 \times 10^{8}\,M^{-1}s^{-1}$) and $k_{TBA,\cdot OH}$ ($6.0 \times 10^{8}\,M^{-1}s^{-1}$) are second-order rate constants of ·OH with 4-CP and TBA, respectively [59]. Other unclear ·OH involved reactions are represented by α. The experimental data were fitted by hyperbolic curve with the equation of $y = 1/ax + b$ (Fig. 7b), where $a = k_{TBA,\cdot OH}/(R^{f}_{\cdot OH}\, k_{4-CP,\cdot OH}\,[4 - CP])$. Then, $R^{f}_{\cdot OH}$ can be calculated to be 1.1×10^{-8} M s^{-1} from Eq. (3). On the other hand, the ·OH concentration at steady state ($[\cdot OH]_{ss}$) during 4-CP degradation was obtained by Eq. (4) [60]. k_{obs} represents the fitted apparent first-order kinetic reaction rate constant in 4-CP degradation, which is $3.4 \times 10^{-4}\,s^{-1}$. Thus $[\cdot OH]_{ss}$ is calculated to be 4.5×10^{-13} M, which are less than five orders of magnitude of $R^{f}_{\cdot OH}$ in the data. This

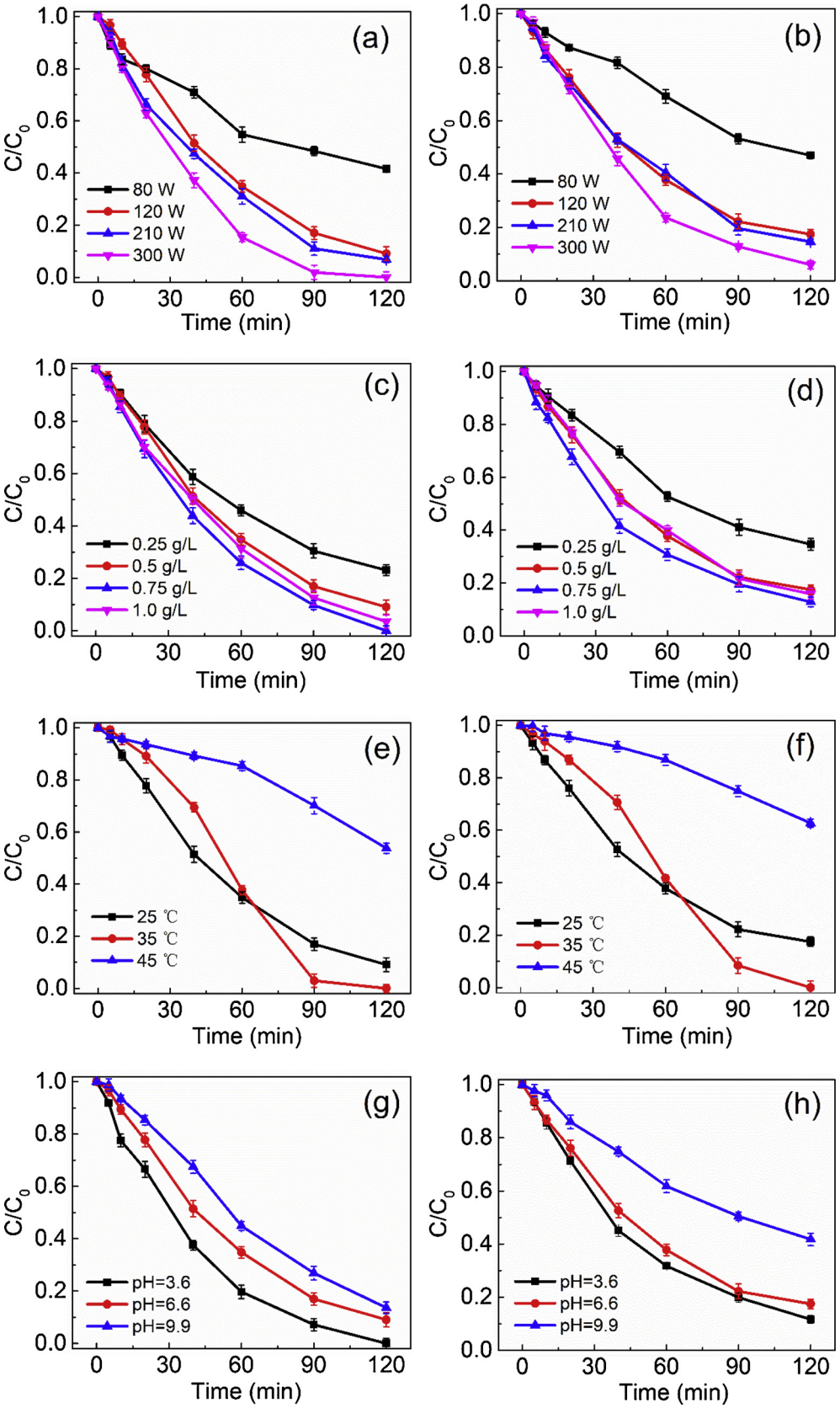

Fig. 5. The removal of 4-CP (a, c, e and g) and Cr(VI) (b, d, f and h) by Au/$BiVO_4$ with different ultrasonic power (a and b); catalyst dosage (c and d); temperature (e and f); and initial pH (g and h).

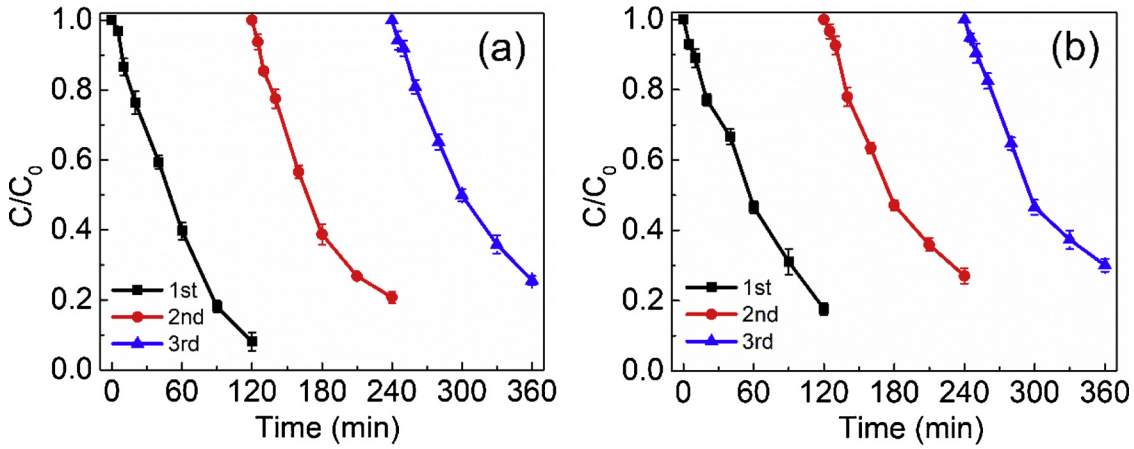

Fig. 6. Recyclability and recovery study of Au/$BiVO_4$ for (a) 4-CP degradation and (b) Cr(VI) reduction.

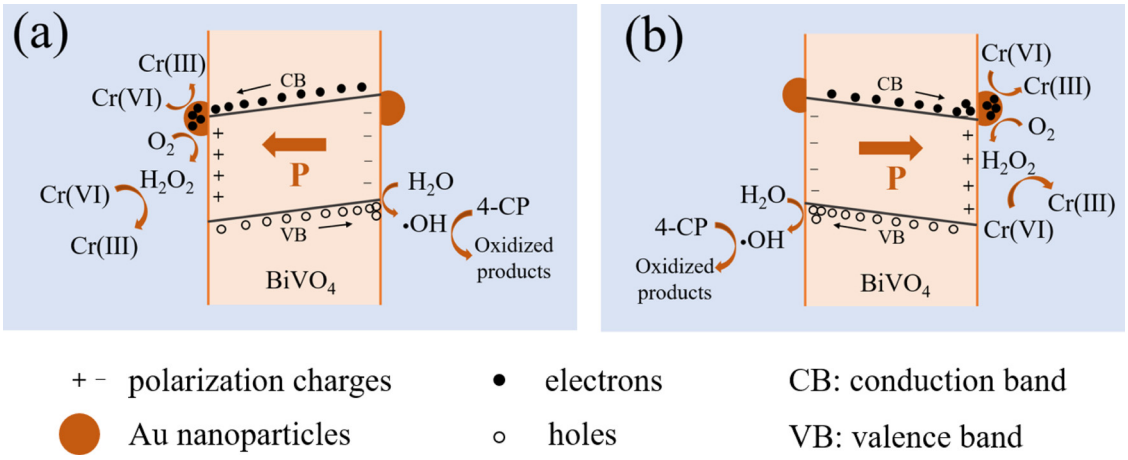

Scheme 1. Proposed mechanism on piezocatalysis of Au/$BiVO_4$.

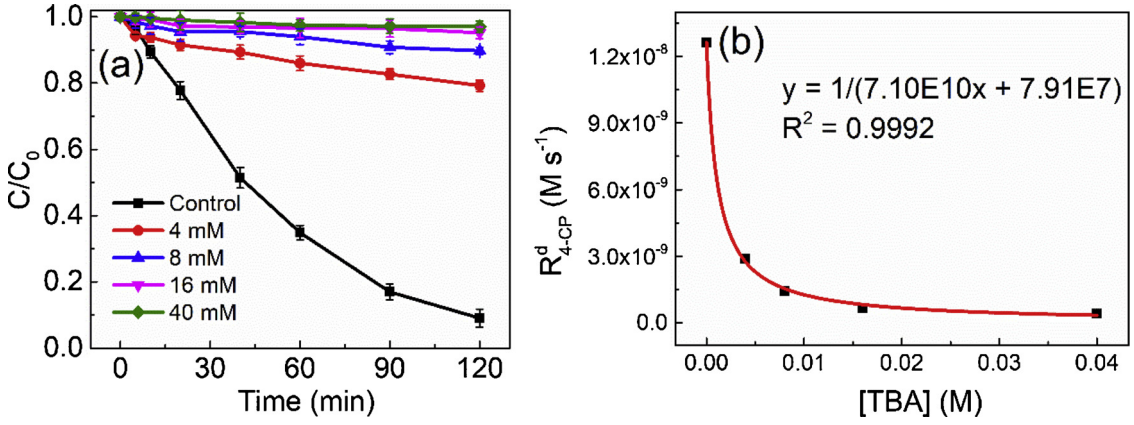

Fig. 7. (a) Effect of TBA concentration on 4-CP degradation; (b) degradation efficiency of 4-CP as a function of TBA dosages.

indicates that the generated ·OH from water oxidation is sufficient to be used for 4-CP degradation in the system.

$$R^d_{4-CP} = (R^f_{\cdot OH}\, k_{4-CP,\cdot OH}\,[4-CP])/(k_{TBA,\cdot OH}\,[TBA] + k_{4-CP,\cdot OH}\,[4-CP] + k_{\alpha\cdot OH}\,[\alpha]) \quad (2)$$

$$R^f_{\cdot OH} = k_{TBA,\cdot OH}/(a \times k_{4-CP,\cdot OH}\,[4-CP]) \quad (3)$$

$$k_{obs} = k_{4-CP,\cdot OH}\,[\cdot OH]_{ss} \quad (4)$$

On the other hand, since the potential of $O_2/O_2^{\cdot -}$ (−0.13 V *vs* NHE) is more negative than the CB potential of Au/$BiVO_4$ (+0.02 V). So, electrons in the CB of Au/$BiVO_4$ cannot reduce the oxygen molecules to produce $O_2^{\cdot -}$, and one-electron reduction of O_2 (Eq. (5)) is thermodynamically prohibited [61]. This is further confirmed by the EPR results that no BMPO−OOH signal can be detected (**Fig. S8**). Thus, the indispensable role of O_2 during piezocatalytic process was probably ascribed to its two-electron reduction (Eq. (6)) and the production of H_2O_2 [61].

$$O_2 + e^- \rightarrow O_2^{\cdot -}\ E = -0.13\,V\ (vs\ NHE) \quad (5)$$

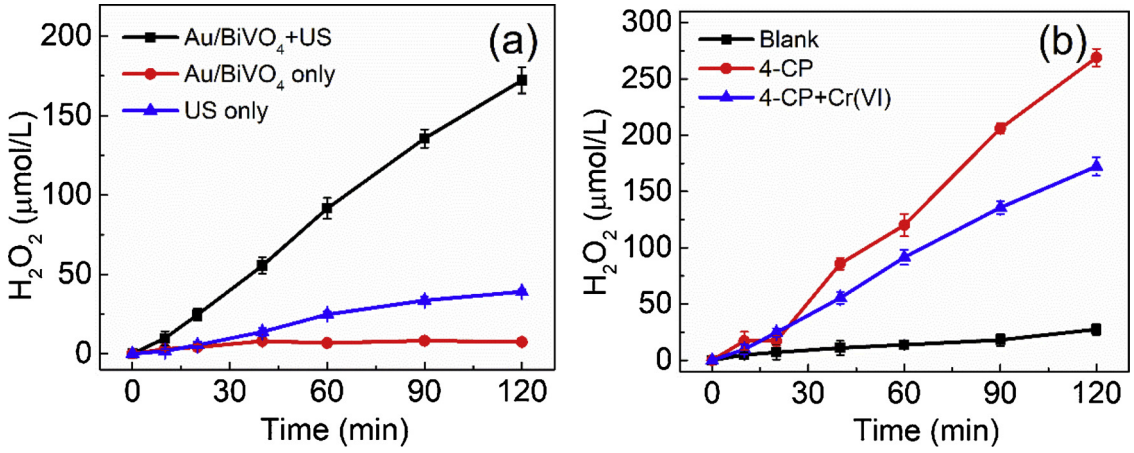

Fig. 8. H_2O_2 accumulation (a) in different processes with both 4-CP and Cr(VI); and (b) with or without 4-CP and Cr(VI) in $Au/BiVO_4$ piezocatalysis.

$$O_2 + 2H^+ + 2e^- \rightarrow H_2O_2\ E = +0.68\,V\ (vs\ NHE) \quad (6)$$

To clarify the piezocatalytic mechanism, the generation and accumulation of H_2O_2 in different conditions were measured. As shown in Fig. 8a, negligible H_2O_2 is produced without ultrasonic vibration, while a minor amount of H_2O_2 (39.0 μmol/L in 120 min) can be detected during ultrasonic vibration in the absence of catalyst. It can be ascribe to that the cavitation effect can make H_2O decompose (Eq. (7)), and H_2O_2 is generated by radical reactions (Eq. (8)) [62]. In the presence of both the catalyst and ultrasonic vibration, the production of H_2O_2 is significantly increased, and its accumulation amount in 120 min reaches 172.2 μmol/L. To clarify the reactions between H_2O_2 and reactants during the piezocatalysis, 0.2 mM H_2O_2 was applied to 4-CP or Cr(VI) solutions in the absence of $Au/BiVO_4$ and ultrasonic irradiation (**Fig. S9**). The degradation of 4-CP by H_2O_2 alone is insignificant, while Cr(VI) can be rapidly reduced after the addition of H_2O_2. It indicates that the reduction of Cr(VI) in the piezocatalytic process is dominated by the generated H_2O_2. The reduction of Cr(VI) by H_2O_2 also proved by H_2O_2 accumulation in different substrates. The absence of Cr(VI) can produce even more H_2O_2 (268.9 μmol/L in 120 min) due to the consumption of H_2O_2 by Cr(VI) (Fig. 8b). The mechanism can also explain the higher removal efficiency of 4-CP and Cr(VI) under acidic conditions (Fig. 5h), since acidic conditions are more conducive to the generation of H_2O_2, which can reduce Cr(VI) and simultaneously accelerate electron-hole separation. As shown in **Fig. S10**, the production of H_2O_2 under acidic, neutral and alkaline conditions are 206.2, 172.2 and 146.3 μmol/L, respectively. The significant production of H_2O_2 at neutral and alkaline conditions can further support the two-electron reduction pathway, because the stability of superoxide radicals, a typical intermediate in the one-electron reduction of O_2, is very poor at pH above 5.0.

$$H_2O \rightarrow \bullet OH + \bullet H \quad (7)$$

$$\bullet OH + \bullet OH \rightarrow H_2O_2 \quad (8)$$

Therefore, the piezocatalytic mechanism of $Au/BiVO_4$ can be summarized in Scheme 1. The excited free electrons on CB can directly react with Cr(VI) and achieving 12% of Cr(VI) reduction (Eq. (9)), while other electrons will react with dissolved oxygen to form H_2O_2 through a two-electron pathway (Eq. (6)), and the generated H_2O_2 acts as a reducing agent to reduce Cr(VI) to Cr(III) (Eq. (10)). Meanwhile, free holes on VB can lead to the reaction with H_2O to form $^{\cdot}OH$ (Eq. (11)), which is capable of oxidize 4-CP molecules into oxidized products (Eq. (12)). As a result, the bifunction of $Au/BiVO_4$ on the simultaneous removal of 4-CP and Cr(VI) is achieved by the piezocatalytic process.

$$Cr(VI) + 3e^- \rightarrow Cr(III)(slow) \quad (9)$$

$$2Cr(VI) + 4H_2O_2 \rightarrow 2Cr(III) + 3O_2 + 6H^+(fast) \quad (10)$$

$$H_2O + h^+ \rightarrow \bullet OH + H^+ \quad (11)$$

$$4-CP + \bullet OH \rightarrow \text{Oxidized products} \quad (12)$$

4. Conclusions

In summary, this study reveals a new piezoelectric material ($Au/BiVO_4$) and employs it as a bifunctional catalyst for simultaneous removal of organic contaminants and heavy metal in an ultrasonic induced piezocatalytic system. The bifunction piezocatalysis on Au modified $BiVO_4$ is realized by the simultaneous removal of 4-CP and Cr (VI) under ultrasonic vibration, achieving 91% of 4-CP degradation and 83% of Cr(VI) reduction in 120 min. Such high performance can be attributed to the internal electric field induced by ultrasonic vibration due to the inherent piezoelectric performance of $Au/BiVO_4$. Hydroxyl radicals and H_2O_2 are revealed to be the main active species for 4-CP oxidation and Cr(VI) reduction, respectively. This work provides more understandings on the piezocatalysis mechanism, and brings a promising strategy to develop efficient piezocatalysts for multiple-target environmental applications.

Declaration of Competing Interest

The authors declare that they have no known competing financial interests or personal relationships that could have appeared to influence the work reported in this paper.

Acknowledgments

Financial supports from the Natural Science Foundation of China (No.21876108) and the National Key Research and Development Program of China (No. 2017YFE9125800) are gratefully acknowledged. We gratefully acknowledge the support in XPS measurements by Dr. Limin Sun of the Instrumental Analysis Center of Shanghai Jiao Tong University.

Appendix A. Supplementary data

Supplementary material related to this article can be found, in the online version, at doi:https://doi.org/10.1016/j.apcatb.2019.118084.

References

[1] Z.L. Wang, Piezopotential gated nanowire devices: piezotronics and piezo-phototronics, Nano Today 5 (2010) 540–552.
[2] S.Y. Lan, J.X. Feng, Y. Xiong, S.H. Tian, S.W. Liu, L.J. Kong, Performance and mechanism of piezo-catalytic degradation of 4-chlorophenol: finding of effective piezo-dechlorination, Environ. Sci. Technol. 51 (2017) 6560–6569.

[3] Y.L. Liu, J.M. Wu, Synergistically catalytic activities of $BiFeO_3/TiO_2$ core-shell nanocomposites for degradation of organic dye molecule through piezophototronic effect, Nano Energy 56 (2019) 74–81.

[4] R.J. Ramalingam, T. Radika, H.A. Al-Lohedan, Preparation and surface characterization of nanodisk/nanoflower-structured gallium-doped zinc oxide as a catalyst for sensor applications, Chin. J. Catal. 37 (2016) 1235–1241.

[5] Z. Liang, C.F. Yan, S. Rtimi, J. Bandara, Piezoelectric materials for catalytic/photocatalytic removal of pollutants: recent advances and outlook, Appl. Catal. B-Environ. 241 (2019) 256–269.

[6] Y.W. Feng, L.L. Ling, Y.X. Wang, Z.M. Xu, F.L. Cao, H.X. Li, Z.F. Bian, Engineering spherical lead zirconate titanate to explore the essence of piezo-catalysis, Nano Energy 40 (2017) 481–486.

[7] M.B. Starr, J. Shi, X. Wang, Piezopotential-driven redox reactions at the surface of piezoelectric materials, Angew. Chem. Int. Ed. 51 (2012) 5962–5966.

[8] J.X. Feng, J.X. Sun, X.S. Liu, J.Z. Zhu, Y. Xiong, S.H. Tian, Enhancement and mechanism of nano-$BaTiO_3$ piezocatalytic degradation of tricyclazole by co-loading Pt and RuO_2, Environ. Sci. - Nano (2019).

[9] W. Lv, L.J. Kong, S.Y. Lan, J.X. Feng, Y. Xiong, S.H. Tian, Enhancement effect in the piezoelectric degradation of organic pollutants by piezo-Fenton process, J. Chem. Technol. Biotechnol. 92 (2017) 152–156.

[10] H.D. Li, Y.H. Sang, S.J. Chang, X. Huang, Y. Zhang, R.S. Yang, H.D. Jiang, H. Liu, Z.L. Wang, Enhanced ferroelectric-nanocrystal-based hybrid photocatalysis by ultrasonic-wave-generated piezophototronic effect, Nano Lett. 15 (2015) 2372–2379.

[11] K.S. Hong, H.F. Xu, H. Konishi, X.C. Li, Direct water splitting through vibrating piezoelectric microfibers in water, J. Phys. Chem. Lett. 1 (2010) 997–1002.

[12] J. Wu, W. Mao, Z. Wu, X. Xu, H. You, A. Xue, Y. Jia, Strong pyro-catalysis of pyroelectric $BiFeO_3$ nanoparticles under a room-temperature cold-hot alternation, Nanoscale 8 (2016) 7343–7350.

[13] S. Singh, N. Khare, Coupling of piezoelectric, semiconducting and photoexcitation properties in $NaNbO_3$ nanostructures for controlling electrical transport: realizing an efficient piezo-photoanode and piezo-photocatalyst, Nano Energy 38 (2017) 335–341.

[14] A. Yourdkhani, G. Caruntu, Characterization of the microstructural and piezoelectric properties of $PbTiO_3$ thin films synthesized by liquid-phase deposition, J. Phys. Chem. C 115 (2011) 14797–14805.

[15] A. Biswas, S. Saha, N.R. Jana, $ZnSnO_3$ nanoparticle-based piezocatalysts for ultrasound-assisted degradation of organic pollutants, ACS Appl. Nano Mater. 2 (2019) 1120–1128.

[16] Z.L. Wang, Progress in piezotronics and piezo-phototronics, Adv. Mater. 24 (2012) 4632–4646.

[17] Y.Z. Zhang, X.L. Huang, J. Yeom, A floatable piezo-photocatalytic platform based on semi-embedded ZnO nanowire array for high-performance water decontamination, Nano-Micro Lett. 11 (2019) 11.

[18] J.M. Wu, W.E. Chang, Y.T. Chang, C.K. Chang, Piezo-catalytic effect on the enhancement of the ultra-high degradation activity in the dark by single- and few-layers MoS_2 nanoflowers, Adv. Mater. 28 (2016) 3718–3725.

[19] J.H. Lin, Y.H. Tsao, M.H. Wu, T.M. Chou, Z.H. Lin, J.M. Wu, Single- and few-layers MoS_2 nanocomposite as piezo-catalyst in dark and self-powered active sensor, Nano Energy 31 (2017) 575–581.

[20] D.K. Shao, L. Zhang, S.M. Sun, W.Z. Wang, Oxygen reduction reaction for generating H_2O_2 through a piezo-catalytic process over bismuth oxychloride, ChemSusChem 11 (2018) 527–531.

[21] K. Wei, K.X. Li, L.S. Yan, S.L. Luo, H.Q. Guo, Y.H. Dai, X.B. Luo, One-step fabrication of g-C_3N_4 nanosheets/TiO_2 hollow microspheres heterojunctions with atomic level hybridization and their application in the multi-component synergistic photocatalytic systems, Appl. Catal. B-Environ. 222 (2018) 88–98.

[22] F.X. Wang, X.H. Yi, C.C. Wang, J.G. Deng, Photocatalytic Cr(VI) reduction and organic-pollutant degradation in a stable 2D coordination polymer, Chin. J. Catal. 38 (2017) 2141–2149.

[23] Y.J. Yao, Y. Hu, M.J. Yu, C. Lian, M.X. Gao, J. Zhang, G.W. Li, S.B. Wang, Nitrogen-doped carbon encapsulating molybdenum carbide and nickel nanostructures loaded with PVDF membrane for hexavalent chromium reduction, Chem. Eng. J. 344 (2018) 535–544.

[24] M. Hua, S.J. Zhang, B.C. Pan, W.M. Zhang, L. Lv, Q.X. Zhang, Heavy metal removal from water/wastewater by nanosized metal oxides: a review, J. Hazard. Mater. 211-212 (2012) 317–331.

[25] J. Bandara, J.A. Mielczarski, A. Lopez, J. Kiwi, 2. Sensitized degradation of chlorophenols on iron oxides induced by visible light - comparison with titanium oxide, Appl. Catal. B-Environ. 34 (2001) 321–333.

[26] X. Bai, Y.Y. Du, X.Y. Hu, Y.D. He, C.L. He, E.Z. Liu, J. Fan, Synergy removal of Cr (VI) and organic pollutants over RP-MoS_2/rGO photocatalyst, Appl. Catal. B-Environ. 239 (2018) 204–213.

[27] Y.C. Deng, L. Tang, G.M. Zeng, Z.J. Zhu, M. Yan, Y.Y. Zhou, J.J. Wang, Y.N. Liu, J.J. Wang, Insight into highly efficient simultaneous photocatalytic removal of Cr (VI) and 2,4-dichlorophenol under visible light irradiation by phosphorus doped porous ultrathin g-C_3N_4 nanosheets from aqueous media: performance and reaction mechanism, Appl. Catal. B-Environ. 203 (2017) 343–354.

[28] Z.F. Huang, L. Pan, J.J. Zou, X.W. Zhang, L. Wang, Nanostructured bismuth vanadate-based materials for solar-energy-driven water oxidation: a review on recent progress, Nanoscale 6 (2014) 14044–14063.

[29] J. Ke, X.G. Duan, S. Luo, H.Y. Zhang, H.Q. Sun, J. Liu, M. Tade, S.B. Wang, UV-assisted construction of 3D hierarchical rGO/Bi_2MoO_6 composites for enhanced photocatalytic water oxidation, Chem. Eng. J. 313 (2017) 1447–1453.

[30] S.M. Sun, W.Z. Wang, D.Z. Li, L. Zhang, D. Jiang, Solar light driven pure water splitting on quantum sized BiVO4 without any cocatalyst, ACS Catal. 4 (2014) 3498–3503.

[31] X.T. Liu, F.Q. Zhang, P.Q. Long, T. Lu, H.R. Zeng, Y. Liu, R.L. Withers, Y.X. Li, Z.G. Yi, Anomalous photovoltaic effect in centrosymmetric ferroelastic $BiVO_4$, Adv. Mater 30 (2018) e1801619.

[32] Z.K. Liu, F. Yan, The application of bismuth-based oxides in organic-inorganic hybrid photovoltaic devices, J. Am. Ceram. Soc. 95 (2012) 1944–1948.

[33] S. Xu, L. Guo, Q. Sun, Z.L. Wang, Piezotronic effect enhanced plasmonic photocatalysis by AuNPs/$BaTiO_3$ heterostructures, Adv. Funct. Mater. 29 (2019) e1808737.

[34] T.M. Chou, S.W. Chan, Y.J. Lin, P.K. Yang, C.C. Liu, Y.J. Lin, J.M. Wu, J.T. Lee, Z.H. Lin, A highly efficient Au-MoS_2 nanocatalyst for tunable piezocatalytic and photocatalytic water disinfection, Nano Energy 57 (2019) 14–21.

[35] M.C. Long, W.M. Cai, J. Cai, B.X. Zhou, X.Y. Chai, Y.H. Wu, Efficient photocatalytic degradation of phenol over $Co_3O_4/BiVO_4$ composite under visible light irradiation, J. Phys. Chem. B 110 (2006) 20211–20216.

[36] M.C. Long, J.J. Jiang, Y. Li, R.Q. Cao, L.Y. Zhang, W.M. Cai, Effect of gold nanoparticles on the photocatalytic and photoelectrochemical performance of Au modified $BiVO_4$, Nano-Micro Lett. 3 (2011) 171–177.

[37] Y.X. Ye, Z. Jiang, Z. Xu, X.L. Zhang, D.D. Wang, L. Lv, B.C. Pan, Efficient removal of Cr(III)-organic complexes from water using UV/Fe(III) system: negligible Cr(VI) accumulation and mechanism, Water Res. 126 (2017) 172–178.

[38] L.H. Zheng, X.J. Yu, M.C. Long, Q.L. Li, Humic acid-mediated visible-light degradation of phenol on phosphate-modified and Nafion-modified TiO_2 surfaces, Chin. J. Catal. 38 (2017) 2076–2084.

[39] J.L. Zhang, Y. Lu, L. Ge, C.C. Han, Y.J. Li, Y.Q. Gao, S.S. Li, H. Xu, Novel AuPd bimetallic alloy decorated 2D $BiVO_4$ nanosheets with enhanced photocatalytic performance under visible light irradiation, Appl. Catal. B-Environ. 204 (2017) 385–393.

[40] C.N. Van, W.S. Chang, J.W. Chen, K.A. Tsai, W.Y. Tzeng, Y.C. Lin, H.H. Kuo, H.J. Liu, K.D. Chang, W.C. Chou, C.L. Wu, Y.C. Chen, C.W. Luo, Y.J. Hsu, Y.H. Chu, Heteroepitaxial approach to explore charge dynamics across Au/$BiVO_4$ interface for photoactivity enhancement, Nano Energy 15 (2015) 625–633.

[41] Y. Zhao, X.Y. Huang, F. Gao, L.L. Zhang, Q.F. Tian, Z.B. Fang, P. Liu, Study on water splitting characteristics of CdS nanosheets driven by the coupling effect between photocatalysis and piezoelectricity, Nanoscale 11 (2019) 9085–9090.

[42] D.F. Yu, Z.H. Liu, J.M. Zhang, S. Li, Z.C. Zhao, L.F. Zhu, W.S. Liu, Y.H. Lin, H. Liu, Z.T. Zhang, Enhanced catalytic performance by multi-field coupling in $KNbO_3$ nanostructures: piezo-photocatalytic and ferro-photoelectrochemical effects, Nano Energy 58 (2019) 695–705.

[43] C.C. Jin, D.M. Liu, J. Hu, Y. Wang, Q. Zhang, L. Lv, F.W. Zhuge, The role of microstructure in piezocatalytic degradation of organic dye pollutants in wastewater, Nano Energy 59 (2019) 372–379.

[44] D.Z. Lu, P.F. Fang, W.H. Wu, J.Q. Ding, L.L. Jiang, X.N. Zhao, C.H. Li, M.C. Yang, Y.Z. Li, D.H. Wang, Solvothermal-assisted synthesis of self-assembling TiO_2 nanorods on large graphitic carbon nitride sheets with their anti-recombination in the photocatalytic removal of Cr(VI) and rhodamine B under visible light irradiation, Nanoscale 9 (2017) 3231–3245.

[45] R.L. Qiu, D.D. Zhang, Z.H. Diao, X.F. Huang, C. He, J.L. Morel, Y. Xiong, Visible light induced photocatalytic reduction of Cr(VI) over polymer-sensitized TiO_2 and its synergism with phenol oxidation, Water Res. 46 (2012) 2299–2306.

[46] W. Liu, W.L. Sun, A.G.L. Borthwick, T. Wang, F. Li, Y.D. Guan, Simultaneous removal of Cr(VI) and 4-chlorophenol through photocatalysis by a novel anatase/titanate nanosheet composite: synergetic promotion effect and autosynchronous doping, J. Hazard. Mater. 317 (2016) 385–393.

[47] R. Zanella, S. Giorgio, C.R. Henry, C. Louis, Alternative methods for the preparation of gold nanoparticles supported on TiO_2, J. Phys. Chem. B 106 (2002) 7634–7642.

[48] S.Z. You, Y. Hu, X.C. Liu, C.H. Wei, Synergetic removal of Pb(II) and dibutyl phthalate mixed pollutants on Bi_2O_3-TiO_2 composite photocatalyst under visible light, Appl. Catal. B-Environ. 232 (2018) 288–298.

[49] M.B. Starr, X.D. Wang, Fundamental analysis of piezocatalysis process on the surfaces of strained piezoelectric materials, Sci. Rep. 3 (2013) e2160.

[50] J. Wang, Z. Jiang, Z.H. Zhang, Y.P. Xie, X.F. Wang, Z.Q. Xing, R. Xu, X.D. Zhang, Sonocatalytic degradation of acid red B and rhodamine B catalyzed by nano-sized ZnO powder under ultrasonic irradiation, Ultrason. Sonochem. 15 (2008) 768–774.

[51] M.R. Li, C. Song, Y. Wu, M. Wang, Z.P. Pan, Y. Sun, L. Meng, S.G. Han, L.J. Xu, L. Gan, Novel Z-scheme visible-light photocatalyst based on $CoFe_2O_4$/BiOBr/Graphene composites for organic dye degradation and Cr(VI) reduction, Appl. Surf. Sci. 478 (2019) 744–753.

[52] L. Tang, G.D. Yang, G.M. Zeng, Y. Cai, S.S. Li, Y.Y. Zhou, Y. Pang, Y.Y. Liu, Y. Zhang, B. Luna, Synergistic effect of iron doped ordered mesoporous carbon on adsorption-coupled reduction of hexavalent chromium and the relative mechanism study, Chem. Eng. J. 239 (2014) 114–122.

[53] Y. Wei, H.R. Su, Y.W. Zhang, L.H. Zheng, Y. Pan, C. Su, W. Geng, M.C. Long, Efficient peroxodisulfate activation by iodine vacancy rich bismuth oxyiodide: a vacancy induced mechanism, Chem. Eng. J. 375 (2019) e121971.

[54] H.L. Liu, Y.P. Ma, J.Y. Chen, M.C. Wen, G.Y. Li, T.C. An, Highly efficient visible-light-driven photocatalytic degradation of VOCs by CO_2-assisted synthesized mesoporous carbon confined mixed-phase TiO_2 nanocomposites derived from MOFs, Appl. Catal. B-Environ. 250 (2019) 337–346.

[55] Y.F. Wang, D. Zhao, H.W. Ji, G.L. Liu, C.C. Chen, W.H. Ma, H.Y. Zhu, J.C. Zhao, Sonochemical hydrogen production efficiently catalyzed by Au/TiO_2, J. Phys. Chem. C 114 (2010) 17728–17733.

[56] J. Wang, T. Ma, Z.H. Zhang, X.D. Zhang, Y.F. Jiang, Z.J. Pan, F.Y. Wen, P.L. Kang, P. Zhang, Investigation on the sonocatalytic degradation of methyl orange in the presence of nanometer anatase and rutile TiO_2 powders and comparison of their sonocatalytic activities, Desalination 195 (2006) 294–305.

[57] W.J. Wang, H.N. Wang, G.Y. Li, T.C. An, H.J. Zhao, P.K. Wong, Catalyst-free

activation of persulfate by visible light for water disinfection: efficiency and mechanisms, Water Res. 157 (2019) 106–118.
[58] Y. Pan, H.R. Su, Y.T. Zhu, H. Vafaei Molamahmood, M.C. Long, CaO_2 based Fenton-like reaction at neutral pH: accelerated reduction of ferric species and production of superoxide radicals, Water Res. 145 (2018) 731–740.
[59] G.V. Buxton, C.L. Greenstock, W.P. Helman, A.B. Ross, Critical review of rate constants for reactions of hydrated electrons, hydrogen atoms and hydroxyl radicals (•OH/•O^-) in aqueous solution, J. Phys. Chem. Ref. Data 17 (1988) 513–886.
[60] J. Brame, M.C. Long, Q.L. Li, P. Alvarez, Trading oxidation power for efficiency: differential inhibition of photo-generated hydroxyl radicals versus singlet oxygen, Water Res. 60 (2014) 259–266.
[61] H. Hirakawa, S. Shiota, Y. Shiraishi, H. Sakamoto, S. Ichikawa, T. Hirai, Au nanoparticles supported on $BiVO_4$: effective inorganic photocatalysts for H_2O_2 production from water and O_2 under visible light, ACS Catal. 6 (2016) 4976–4982.
[62] Y.F. Wang, D. Zhao, W.H. Ma, C.C. Chen, J.C. Zhao, Enhanced sonocatalytic degradation of azo dyes by Au/TiO_2, Environ. Sci. Technol. 42 (2008) 6173–6178.